Journal of Energy Storage 91 (2024) 112087

Contents lists available at ScienceDirect

Journal of Energy Storage

journal homepage: www.elsevier.com/locate/est

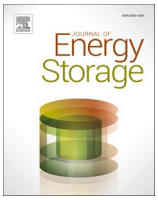

Research Papers

A technique for separating the impact of cycle aging and temperature on Li-ion battery capacity

Simone Barcellona [a,*], Lorenzo Codecasa [a], Silvia Colnago [b], Christian Laurano [a], Luigi Piegari [a], Sergio Toscani [a]

[a] Department of Electronics, Information and Bioengineering, Politecnico di Milano, Italy
[b] Department of Generation Technologies and Material, Ricerca sul Sistema Energetico S.p.A., Milan, Italy

ARTICLE INFO

Keywords:
Lithium-ion battery
Battery electrical model
Cycle aging
Capacity fade

ABSTRACT

Reduction of battery capacity is a well-known symptom of aging, making it a universally accepted indicator of the state of health. Capacity also significantly depends on temperature, therefore, separating the effect of temperature from that due to aging has utmost important for a proper state of health assessment. However, according to the latest literature, there is a lack of information about how the temperature dependency of capacity changes with battery aging. In this respect, the study presented in this paper is based on an experimental campaign aimed at measuring battery capacity at different temperatures and cycling levels. Starting from the obtained results, an analytical model describing how the variation law of battery capacity with temperature is affected by cycling was proposed and validated. The achieved accuracy is better than 0.6 % for all the considered operating conditions.

1. Introduction

In the market, many types of rechargeable batteries based on different chemistries are currently available. At present, lithium-ion batteries (LiBs) are the most widely employed in multifold applications, covering a broad range of power and capacity. The main reason is that such technology ensures high energy density, high power density, remarkable efficiency, low self-discharge, no memory effect, and long expected lifetime [1,2], resulting in a favorable performance-to-cost ratio. In any case, these applications can mainly be classified as stationary and mobile. In the former, LiBs can be used, for instance, as storage systems integrated with the electric grid to support non-programmable renewable energy sources, or inside uninterruptible power supply systems for supplying critical loads [3]. In mobile applications, LiBs are used as sources of energy and they can be extensively found in electronic devices (such as laptops, smartphones, tablets, etc.), electromedical equipment (including defibrillators, pacemakers, and so on), in electric vehicles, or in the aerospace sector [4–6].

The overall performance of a battery is mainly expressed in terms of maximum stored energy (related to the battery capacity) and the maximum electric power that can be exchanged (related to the battery internal resistance). These aspects are very important to guarantee the required performance in all the applications.

Unfortunately, LiBs experience different aging mechanisms, in particular those due to the passage of time under predetermined environmental conditions (defined as calendar aging) and the repetitive charge and discharge cycles they undergo during usage (defined as cycle aging) [7,8]. Depending on the type of aging mechanism, battery degradation can lead to a decrease in its capacity (energy fade) or an increase in its internal resistance (power fade). To cope with these degradation mechanisms and ensure optimal operating conditions, it is of paramount importance to develop proper battery models. This enables batteries to operate within safe and optimal working ranges. The integration of such models into battery management systems is crucial, as they enable estimating important battery parameters such as state of charge (SOC) and state of health (SOH) [9]. Various battery models addressing electric, thermal, and aging aspects, either individually or coupled can be found in the literature. Furthermore, these models may adopt physical, analytical, or circuital approaches [10]. In particular, among the electric models those based on the circuital approach are extremely flexible and enable reaching the desired trade-off between complexity and accuracy [11]. Moreover, they can be as simple as those in [12,13], or more complicated, as in [14–16]. Selecting the suitable model depends on the desired level of accuracy and the specific phenomena that need to be considered, according to the peculiar application.

* Corresponding author.
E-mail address: simone.barcellona@polimi.it (S. Barcellona).

https://doi.org/10.1016/j.est.2024.112087
Received 13 November 2023; Received in revised form 28 February 2024; Accepted 12 May 2024
Available online 18 May 2024

The SOH of an LiB is typically quantified in terms of capacity fade or power fade with respect to those measured as the battery was new. Conventionally, the battery is considered at its end of life, when its capacity falls below 80 % of its initial value or its internal resistance doubles [17]. In this work, the focus will be on the reduction of battery capacity as aging indicator.

It is worth to note that the term "capacity" typically refers to the electric charge that can be stored in the battery. Therefore, battery capacity can be easily measured by time-integrating the battery current during a full charge or discharge under fixed conditions [18]. Several technical commissions and standardization organizations have proposed reference procedures for capacity measurements, such as those reported in [17,19,20]. For example, ISO [20] recommends to discharge high-power batteries at 1C.

It is well-known that battery capacity strongly depends on temperature [21–24]. In this respect, the study conducted in [22] analyzed the variation of battery capacity with respect to temperature, and the experimental results were fitted with a third-degree polynomial function. Nevertheless, the analysis was carried out only for a fresh LiB cell. On the other hand, in the literature, several research works analyze how battery capacity decreases with time and cycling. A comprehensive review of the different aging models can be found in [10]. Calendar aging mostly depends on the time evolution of the storage temperature and SOC [25]. Cycle aging is mainly affected by operating temperature, depth of discharge, voltage limits, and current rate as a function of the number of full equivalent cycles or total moved charge [26–32]. In [25], the authors analyzed how battery capacity is affected by calendar aging at different storage temperatures and SOC levels. In [26], many LiB cells were cycled under various conditions, in terms of charging/discharging current rates, maximum cut-off voltages, and depths of discharge. The study demonstrated how capacity decreases as a function of the number of cycles according to these influence factors. Conversely, in [33] the authors showed that the shape of cycles does not affect capacity fade between the 20 % and 80 % of SOC. Additionally, in [34], the authors demonstrated that, for given operating conditions, battery current rate does not affect capacity fade. In [29], the authors studied the influence of temperature on battery capacity, considering cycle aging over 25 °C to 55 °C temperature range.

Nevertheless, it is worth noting that, for a given cycling level, some battery parameters, such as its capacity and internal resistance, generally exhibit dependency on some of the same factors affecting the aging process. Indeed, temperature, SOC, voltage, and current rate do not just affect the actual value of capacity or internal resistance for a given aging condition, but they also impact the aging process. Therefore, directly inferring the SOH from capacity and resistance measurements is reliable only if such measurements are performed under predetermined reference conditions in terms of the aforementioned influence factors. In fact, under these assumptions, many aging models proposed in the literature can be adopted to predict the capacity reduction and internal resistance increase as a function of time and cycling. From a different point of view, there are several research works that analyze how the capacity and internal resistance of a battery change as a function of the same influence factors for a fixed cycling level (typically fresh battery cells). However, there seems to be a lack of information regarding how these variation laws change as a function of cycling.

Nevertheless, concerning internal resistance, in a previous work [35], the authors analyzed how the variation law of the battery internal resistance dependency on temperature and SOC changes with cycling. Regarding battery capacity, in [36], the authors compared two LiB cells, one fresh and the other aged through cycling at 35 °C. The voltage responses of the two LiB cells were measured during discharge at different temperatures and current rates. In [37], the authors aged an LiB cell by performing several aging cycles at 3C and 50 °C. After 300 cycles and 600 cycles, they measured the discharge capacity at different temperatures ranging from −10 °C to 45 °C. A similar analysis was performed in [38], where the LiB cell was aged at 5C and 40 °C. In [39], the authors performed capacity measurements for each temperature between 0 °C and 40 °C, with a 2 °C step. The procedure was repeated four times to observe the capacity-temperature behavior for different aging cycles.

However, there is a lack of a thorough analysis about how the law of capacity variation with temperature changes during cycling. In particular, in [39], the capacity was measured for the different temperatures during the cycle aging process, thus without decoupling the two effects. Nevertheless, this aspect is of key importance, as far as the reduction of battery capacity is used as an SOH indicator; temperature dependency may jeopardize the outcome if it is not properly considered.

In this respect, similar to the analysis conducted in [35] for the battery internal resistance, the aim of the present paper is to study how the variation law of battery capacity as a function of temperature changes with battery cycling. Unlike [22], this variation law was modeled using a different analytical expression based on a double exponential function. In particular, the capacity of the battery cell under test was estimated by integrating the current during discharge processes at different temperatures in a range between 20 °C and 50 °C. Furthermore, the battery cell was aged through several charging/discharging cycles under fixed conditions in terms of temperature and current rate. Therefore, the capacity of the battery was measured at the beginning of its life and after each group of aging cycles.

2. Electric battery model

For the purpose of the present analysis, the third-order Thevenin circuit model [40], shown in Fig. 1, was adopted. It consists of an ideal voltage source connected in series with a resistor and three parallel RC branches. The ideal voltage source, V_{OC}(SOC), represents the open circuit voltage (OCV) of the battery, and it is related to the stored energy, thus reflecting the battery capacity. The OCV is also affected by several other factors such as battery chemistry, SOC, temperature, and aging. The series resistor, R_s, models the electronic resistance of the current collectors and electrodes, as well as the ionic resistance of the electrolyte; it is the so-called high-frequency resistance of the battery. The other terms enable modeling the medium- and low-frequency behavior of the battery and are related to different slow-dynamic phenomena. The resistor R_{SEI} and capacitor C_{SEI} model the resistance and capacitance effect of solid electrolyte interface; the resistor R_{ct} and capacitor C_{dl} model the charge transfer process and double layer effect, respectively; finally, the resistor R_d and capacitor C_d model the resistance and capacitance effects of lithium/lithium-ion diffusion processes into the electrode/electrolyte.

It is worth noting that, under steady state conditions, the total internal resistance of the battery corresponds to the sum of the four resistive contributions. The estimation of the latter is important to properly compare the battery capacities under different conditions in terms of temperature and cycling levels, as will be elucidated later.

By definition, calendar aging is purely a function of time for given storage conditions. On the contrary, cycle aging is the result of multiple charges and discharges, therefore it is considered as a function of the number of equivalent cycles performed under predetermined reference conditions, or of the total moved charge Q, defined as:

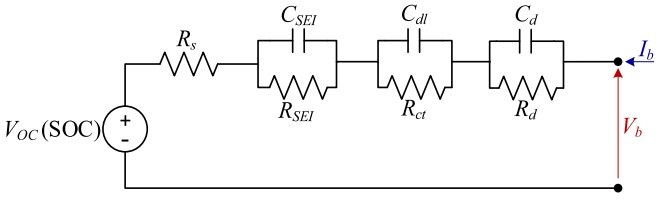

Fig. 1. Equivalent electric circuit of LiB.

$$Q = \int_0^t |I_b(\tau)|\, d\tau. \quad (1)$$

Moreover, [33,34] show that, under given environmental conditions, the moved charge directly affects the aging level (the reduction of battery capacity C, typically expressed in Ah [20]), and it is weakly affected by discharge depth as well as battery current.

On the other hand, the battery capacity C, was measured following the procedure adopted in [22] through the constant current-constant voltage (CC-CV) protocol during charging and CC during discharging. Specifically, the CC-CV protocol consisted of fully charging the battery at a constant current of 1C until reaching the maximum cut-off voltage. This voltage was then maintained until the current decayed below 0.5C, thus, according to Fig. 1, the voltage drops over the internal resistances can be considered nil, ensuring that 100 % SOC was reached. Then, the battery was fully discharged at a constant current of 1C until reaching the minimum cut-off voltage, while measuring the battery current, I_b. Therefore, the battery capacity was obtained as:

$$C = \int_{t_{max}}^{t_{min}} I_b(\tau) d\tau \quad (2)$$

where t_{max} and t_{min} are the initial and final time instants corresponding to the maximum and minimum cut-off voltages related to the discharge, respectively.

In this respect, during the charging, the maximum cut-off voltages corresponded to the maximum OCVs for all the tests. However, even though the discharge current was the same for all the tests, the internal resistance of the battery varies with SOC, temperature, and cycle aging. Consequently, the resulting voltage drop across the internal resistance was different according to the operating conditions. Therefore, if one directly considered the values of the battery capacity obtained by integrating the battery current up to the minimum cut-off voltage, they would correspond to different minimum OCVs, because of the varying internal resistance values, making the capacity values not comparable. According to [22], the internal resistance also affects capacity; the reason is that capacity was evaluated by integrating the battery current during discharge at 1C, but without removing the effect of the internal resistance. Therefore, for the sake of a fair comparison, capacity values corresponding to the same minimum OCVs must be considered. On the other hand, compensating for the internal resistance ensures the consistency of the obtained capacity values, thus leading to a more significant comparison. For the purpose, one may evaluate the internal resistance of a fully discharged battery for each temperature and aging condition, remove the corresponding voltage drop at the end of the discharge process, and consider the maximum between the OCVs as the minimum cut-off voltage in Eq. (2) for all tests conducted at different temperatures and cycling levels. To do this, according to the electric circuit depicted in Fig. 1, when a current step is applied to the battery, an electric transient occurs according to the different time constants due to the different RC branches. Specifically, the largest one is due to the diffusion process. Since the battery discharge was performed at a constant current of 1C, it is possible to assume steady-state conditions as the voltage reaches the minimum cut-off value, thus capacitors can be considered as open circuits. In this way, when the battery voltage reaches the minimum cut-off value, a 1C current step occurs, which can be employed to evaluate the internal resistance using the dc current pulse method [41].

3. Experimental activity

The battery cell employed in this work was a lithium cobalt oxide (LCO) cell 8773160K manufactured by General Electronics Battery Co. Ltd., whose main parameters are reported in Table 1.

Table 1
Battery cell specifications.

Parameter	Value	Units
Rated capacity	10	Ah
Rated voltage	3.7	V
Charge cut-off voltage	4.2	V
Discharge cut-off voltage	2.75	V
Maximum continuous discharge current	100 (10C)	A
Maximum peak discharge current	150 (15C)	A

3.1. Experimental setup

Experiments were conducted using a Biologic Science Instruments 100 A booster (VMP3B-100) in conjunction with a potentiostat (SP-150), controlled by a PC running EC-LAB software, whose specifications are reported in Table 2. The overall test arrangement is depicted in Fig. 2.

Ensuring uniform and stable battery temperature throughout the tests is of paramount importance. Typically, experiments for evaluating temperature dependency are carried out using a climatic chamber. However, the drawback is that while it ensures a fairly constant ambient temperature, it fails to maintain a steady battery temperature under different operating conditions, mostly because of the slow thermal dynamics with respect to self-heating phenomena. For this reason, three Peltier cells were electrically connected in series and placed between the battery and a properly sized heatsink. Therefore, regulating the current flowing through the Peltier cells enabled a more direct and thus faster control of battery temperature. The proportional-integral temperature control loop was implemented on an F28069M microcontroller from Texas Instruments driving an DRV8323RX inverter from the same manufacturer, which imposes the current of the Peltier cells through pulse width modulation. The battery temperature was measured with a thermocouple placed on the battery surface exposed to air. In this way, the measured temperature, used as feedback for the control, was not affected by the temperature of the Peltier cell. Since the battery is very thin, it is possible to consider temperature as uniform along thickness.

3.2. Test procedure

Fig. 3 shows the block diagram of the adopted experimental procedure, which consisted of two phases: the capacity measurement phase and the cycle aging phase. A preliminary capacity measurement phase was conducted to determine the initial battery capacity, followed by subsequent measurements after each cycle aging phase to assess the capacity reduction corresponding to about 10 kAh, 15 kAh, and 20 kAh of moved charge.

3.3. Capacity measurement phase

Considering the typical battery applications (including automotive, storage, and portable electronics) the ambient temperature could be significantly lower than 20 °C. Nevertheless, during regular operation,

Table 2
Test setup specifications.

SP-150 specifications	
Voltage range	±10 V
Current range	±0.8 A
Voltage measurement accuracy	<10 mV
Current measurement accuracy	<0.8 mA
VMP3B-100 specifications	
Voltage range	0–5 V
Current range	±100 A
Voltage measurement accuracy	<10 mV
Current measurement accuracy	1 A
Impedance measurement accuracy	1 %, 1°

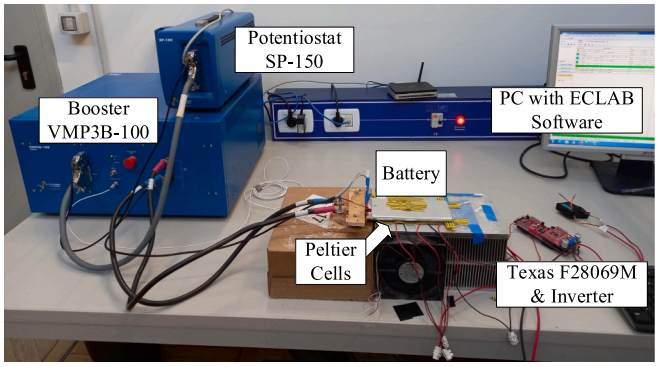

Fig. 2. Adopted test setup.

the battery temperature is generally higher than this value due to self-heating, typically ranging between 15 and 40 °C [42]. Therefore, in this work, battery capacity was evaluated at eight reference temperatures between 20 and 50 °C (i.e., 20 °C, 22.5 °C, 25 °C, 27.5 °C, 30 °C, 33.5 °C, 38 °C, and 46 °C). In practice, because of the limitations of the temperature control loop, measurements were conducted in a range of ±2 °C around the reference values.

Initially, the battery cell was charged to achieve a SOC of 100 % using a CC-CV protocol. In more detail, the battery cell was charged at a rate of 10 A (1C) until the maximum cut-off voltage of 4.2 V was reached, followed by the application of the same voltage until the battery current decayed to 100 mA (0.01C). In turn, the cell was fully discharged with 10 A (1C) current until reaching the minimum cut-off voltage of 2.75 V. The consequent current interruption corresponded to a −10 A (−1C) current step. After this, the battery was left to rest for 1 h, measuring the subsequent voltage transient resulting from relaxation phenomena. The internal resistance was then calculated as the ratio between the voltage change over 1 h and the current step. After evaluating the resistance of the fully discharged battery, the battery cell was charged back to 100 % of SOC, and the same procedure was repeated for the other temperatures.

3.4. Cycle aging phase

Each cycle aging phase consisted of a constant current charge and discharge at a reference temperature of 30 °C. For speeding up the test process, a charge and discharge current of 5C was selected. However, given that battery capacity decreases with aging, the current was reduced to 4C after reaching $Q = 10$ kAh to mitigate the effects of high-frequency aging [43]. This change in the current rate does not impact on the results, as previous findings in [34] indicates that the current rate does not impact aging. In any case, the charge and discharge cycles were limited by two constraints: the SOC was bounded between 20%and 80 %, while the battery voltage was confined within 3.45 V and 4.05 V. It is worth highlighting that if the voltage limits are reached before reaching the SOC bounds, the moved charge within a single cycle would be <6 Ah. Nonetheless, the outcomes presented in [33] demonstrates that battery aging depends on the moved charge, regardless of the cycle shape.

4. Experimental results

The experimental results enable tracking the variation of battery capacity, C, at different temperatures and cycling levels. For a given aging condition, experimental results show that C initially rises with temperature. The behavior could be explained since, according to the Arrhenius equation, reaction rate increases with temperature [44]. This facilitates the intercalation/deintercalation process, leading to increased battery capacity. Furthermore, higher temperatures enhance the concentration and mobility of lithium ions in the electrolyte, making them more prone to intercalation/deintercalation. Therefore, we modeled this behavior with an exponential term in temperature, namely assuming an Arrhenius-like behavior.

However, capacity measurements exhibit significantly lower values at the highest temperature setpoint, which is not explained according to previous considerations. One possible reason is that further increasing the temperature produces excessive movement of lithium ions, making the intercalation/deintercalation process more difficult [22]. To also consider this phenomenon, a second exponential term was introduced, thus resulting in the following expression for battery capacity:

$$C(T) = a \cdot e^{b \cdot T} + c \cdot e^{d \cdot T} + f \tag{3}$$

where a, b, c, d, and f are the fitting coefficients that depend on the cycle aging, while e is the Euler's number. For each cycling level, the corresponding coefficients were estimated by minimizing the Euclidean norm of the deviation between experimental data and the corresponding model output, thus resulting in a nonlinear least-squares problem. Fig. 4 shows the comparison between experimental capacity and model output for each of the four cycling levels, Q.

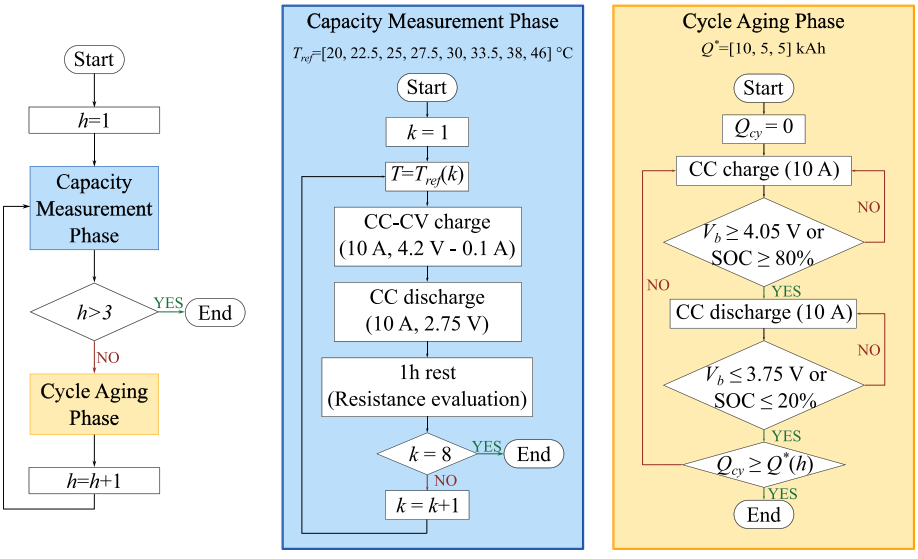

Fig. 3. Block diagram of the experimental test procedure.

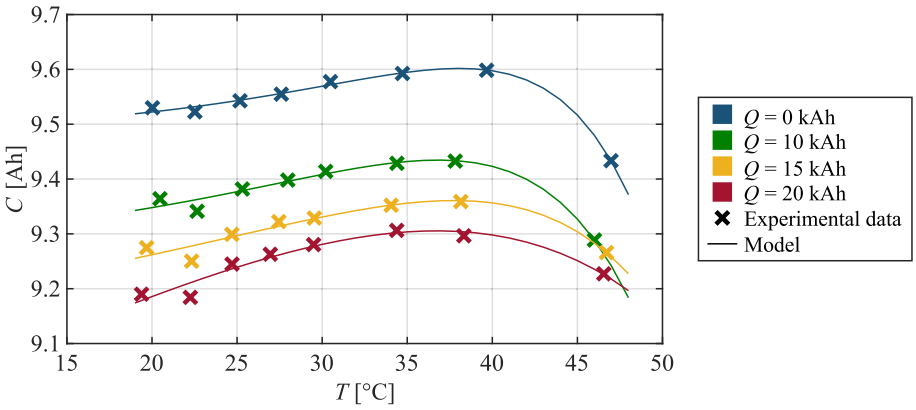

Fig. 4. Experimental and modeled capacity as a function of temperature for different cycling levels using Eq. (3).

The trends reported in Fig. 4 confirm that the proposed fitting expression (3) accurately fits the experimental capacity for all cycling levels. It is interesting to note that battery capacity exhibits a similar trend for all cycling levels. It increases with temperature up to about 40 °C, after which it begins to decrease. An exponential term in Eq. (3) allows a proper fitting of the ascending part of $C(T)$ for each cycling level. On the other hand, the second exponential term enables considering the plateau observed around 35 °C, as well as the decreasing part of $C(T)$. Notably, the reduction in capacity at the highest temperature appears to be more significant at lower cycling levels. Furthermore, capacity values for cycling levels of 10, 15, and 20 kAh are rather close but remarkably different with respect to that measured for the fresh cell.

Examining Fig. 4, it is evident that all four fitting curves exhibit a noticeable deviation from the experimental data at 22.5 °C. Additionally, the curves corresponding to moved charges of 10 kAh and 15 kAh intersect at high temperatures. It is important to note that we are attempting to describe relatively small capacity variations, while batteries are complex electrochemical systems influenced by numerous factors and second-order effects that are challenging to model. Consequently, these small capacity variations are inherently subject to significant uncertainty. Nonetheless, the deviations between experimental data and fitting remain relatively small compared to the overall variation of battery capacity. Additionally, Table 3 reports the corresponding coefficients of determination, R^2, and the normalized root mean square errors (NMRSEs), normalized with respect to the root mean square value of the experimental capacity, confirming the goodness of fit.

Fig. 5 shows the five fitting coefficients of Eq. (3) as functions of the moved charge, which corresponds to the cycling level.

When considering the overall trend of battery capacity as reported in Fig. 4, from a holistic point of view, the qualitative behaviors of the curves are rather similar, with the exception of the curve related to $Q =$ 10 kAh, which crosses the other curves (likely due to a possible error in its last data point). This observation suggests rewriting Eq. (3) under the assumption that the exponents are consistent across all curves, and the three terms are just scaled by three factors, namely $k_1(Q)$, $k_2(Q)$, and $k_3(Q)$, which account for the dependency on cycle aging. This yields the following expression:

$$C(T,Q) = k_1(Q)\cdot a(0)\cdot e^{b(0)T} + k_2(Q)\cdot c(0)\cdot e^{d(0)T} + k_3(Q)\cdot f(0). \tag{4}$$

In Eq. (4) $a(0)$, $b(0)$, $c(0)$, $d(0)$ and $f(0)$ are the parameters modeling the $C(T)$ characteristic of the fresh cell (hence $Q = 0$), which can be obtained by solving a nonlinear least squares problem as previously done with Eq. (3). The scale factors k_1 and k_2 are related to the ascending and descending parts of the curve $C(T)$, while k_3 is an offset term. In this way, it was possible to decouple and quantify the effect of cycle aging separately on the ascending and descending parts of the curve $C(T)$. Furthermore, given the initial values of $a(0)$, $b(0)$, $c(0)$, $d(0)$, and $f(0)$, the scaling factors could be estimated from experimental data by solving a different linear least squares minimization problem for each considered value of Q. This would make it possible to predict the variation of battery capacity with temperature for a given cycling level.

Fig. 6 shows the comparison between the experimental and modeled data for the four cycling levels using the new model (4), which still accurately fits the experimental points for all temperatures and cycling levels, in particular when considering the inherent uncertainty of the experimental data.

Additionally, Table 4 represents the corresponding coefficients of determination, R^2, and NRMSEs which confirm the overall goodness of fit, despite slightly lower values of R^2 in case of significant aging. The reason is that the new fitting problem introduces constraints involving different cycling levels (thus resulting in less degrees of freedom), while the previous approach considers an independent data fitting for each curve. Fig. 7 shows the three scale factors, k_1, k_2, and k_3, as a function of the moved charge. In this case, the coefficient k_3 exhibits a virtually linear trend with respect to Q, while the coefficients k_1 and k_2 do not show a well-defined trend, but they remain relatively constant.

Nonetheless, it would be interesting to introduce a more complete aging model, capable of estimating how the variation law of battery capacity with temperature changes with respect to the overall moved charge. To achieve this, another fitting problem could be formulated by assuming that the three coefficients of Eq. (4) exhibit a linear trend with the moved charge, Q, modeled by introducing the new coefficients m_i and q_i, $i \in \{1,2,3\}$. Therefore, we have

$$\begin{aligned} k_1(Q) &= m_1 Q + q_1 \\ k_2(Q) &= m_2 Q + q_2 \\ k_3(Q) &= m_3 Q + q_3 \end{aligned}. \tag{5}$$

Substituting Eq. (5) into Eq. (4), we obtain

$$C(T,Q) = (m_1 Q + q_1)\cdot a(0)\cdot e^{b(0)T} + (m_2 Q + q_2)\cdot c(0)\cdot e^{d(0)T} + (m_3 Q + q_3)\cdot f(0). \tag{6}$$

Assuming that $a(0)$, $b(0)$, $c(0)$, $d(0)$, and $f(0)$ have been previously computed from the temperature behavior of a fresh battery cell, using Eq. (5) and the experimental data enables the formulation of a new linear least squares minimization problem, whose solution provides the estimates of m_i and q_i. Table 5 reports the obtained values, while Fig. 8 shows the comparison between the experimental and modeled data obtained through Eq. (6) for the four cycling levels. Assuming that the

Table 3
R^2 and NMRSE for the different cycling levels using the model fitting Eq. (3).

Q [kAh]	R^2	NMRSE [%]
0	0.9900	0.2623
9.7	0.9666	0.4477
14	0.9055	0.6421
19	0.9367	0.6280

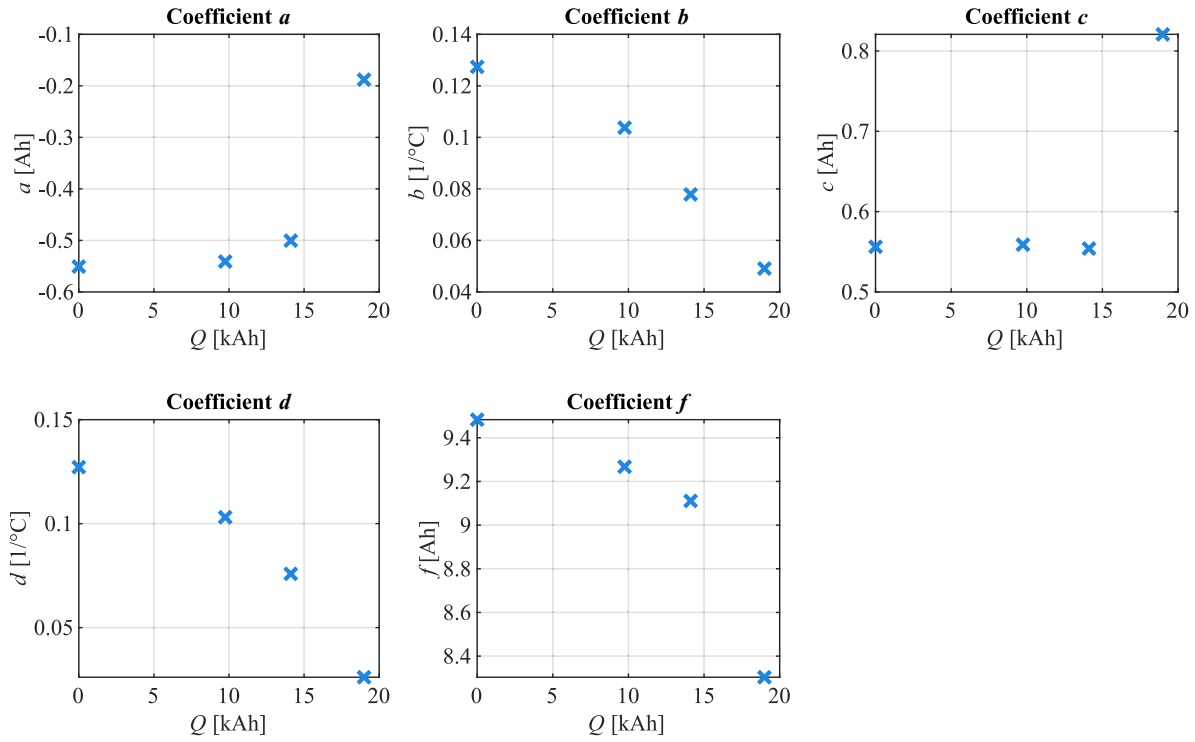

Fig. 5. Fitting coefficients of Eq. (3).

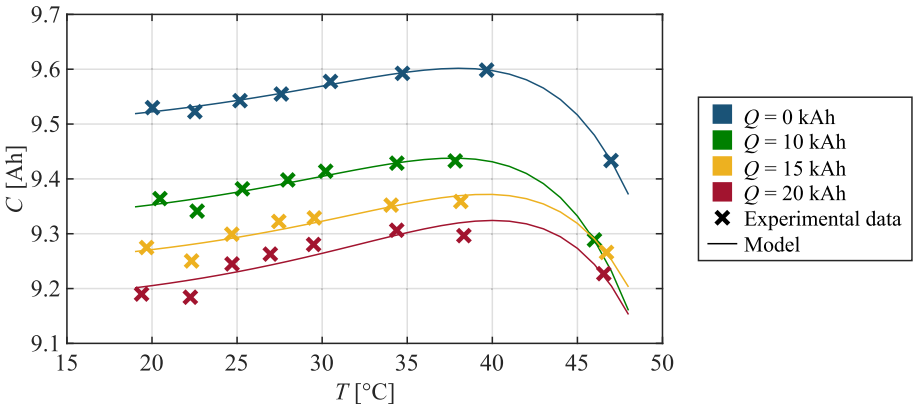

Fig. 6. Experimental and modeled capacity as a function of temperature for different cycling levels using Eq. (4).

Table 4
R^2 and NMRSE for the different cycling levels using the model fitting Eq. (4).

Q [kAh]	R^2	NMRSE [%]
0	0.9900	0.2623
9.7	0.9579	0.5030
14	0.8700	0.7532
19	0.8043	1.104

scaling factors are linearly dependent on Q leads to a stiffer model. Despite the slight degradation observed at the highest cycling level, the overall quality of the fit remains robust, even when considering the uncertainty inherent in the experimental data. This is evidenced by the coefficient of determination, which equals 0.9761, greater than the one obtained for $Q = 10$ kAh using fitting model (4). Additionally, the NRMSE is 1.427 %, further confirming the goodness of fit. It is important to note that while a more complex expression could potentially yield a seemingly better fit by accommodating additional dependencies of the scaling coefficients on Q, such an approach risks overfitting, namely the model just better follows the error contributions.

Finally, to evaluate the accuracy of the proposed model, the relative error of the modeled battery capacity was calculated as follows:

$$e_{rel}(Q,T) = \frac{\left|C_{exp}(Q,T) - C_{mod}(Q,T)\right|}{C_{exp}(Q,T)} \tag{7}$$

where $C_{exp}(Q,T)$ and $C_{mod}(Q,T)$ are the experimental and modeled battery capacity, respectively, for a given temperature or cycling level. From Fig. 9, it is possible to recognize that the error is generally below 0.4 % for all the considered values of temperature and moved charge, confirming the overall good accuracy of the proposed aging model. The two deviations exceeding 0.4 % are likely to be due to the uncertainty of the experimental results.

Indeed, while the quality of the fitting achieved with the proposed aging model is slightly worse than that obtained by considering the cycling levels separately, the errors are small enough for estimating battery capacity at different temperatures and cycling levels, by

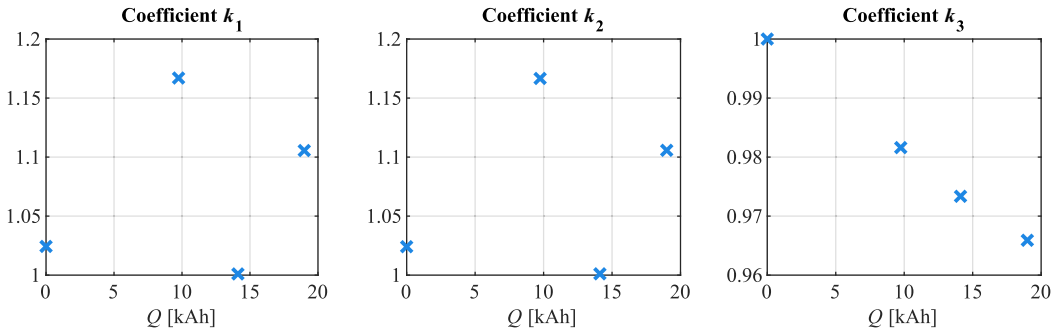

Fig. 7. Fitting coefficients of Eq. (4).

Table 5
Coefficients of Eq. (5).

Coefficient	Value
m_1	$6.284 \cdot 10^{-6}$ Ah^{-1}
q_1	0.9978
m_2	$6.307 \cdot 10^{-6}$ Ah^{-1}
q_2	0.9975
m_3	$-1.839 \cdot 10^{-6}$ Ah^{-1}
q_3	1.000

exploiting the knowledge about the battery capacity variation law with temperature for a fresh battery cell.

5. Conclusion

The decrease of capacity with cycle aging is one of the most important factors that limits the lifespan of batteries. Moreover, while many research works have analyzed the effect of temperature on the variation of battery capacity, the impact of cycle aging on the relationship between battery capacity and temperature has not been studied in detail, although it is of paramount importance for a more accurate SOH assessment. In this respect, the present work investigated the dependency of the capacity of an LCO battery on both temperature and cycle aging. In particular, the battery under test was cycled for about 20 kAh under fixed temperature conditions of 30 °C. At the beginning of the battery life and after each cycle aging phase, the battery capacity was evaluated at eight different temperatures.

Firstly, for each cycling level, the experimental data of the battery capacity at the different temperatures were fitted using the proposed model Eq. (3). This model consists of two exponential terms and one constant term, resulting in a total of five fitting coefficients computed with the least squares approach. The results show a good match between the experimental and modeled data across all temperatures and cycling levels.

Upon observing the experimental data, the model was refined to describe also how the dependency between capacity and temperature changes with cycle aging, starting from that measured on a fresh cell. This involved multiplying each term representing the behavior of the fresh cell by a scale factor dependent on aging. This approach enables the separate quantification of the effect of cycle aging on the ascending and descending parts of the capacity-temperature curve. Additionally, it was observed that the variation of these coefficients could be assumed as linear with the moved charge, expressed through a set of six coefficients estimated using the least squares approach. The comparison between the experimental and modeled data confirms the overall good accuracy of the proposed aging model, with a percentage error in estimated capacity below 0.6 % for all explored conditions.

Funding

The work of Silvia Colnago has been financed by the Research Fund for the Italian Electrical System under the Three-Year Research Plan 2022–2024 (DM MITE n. 337, 15.09.2022), in compliance with the

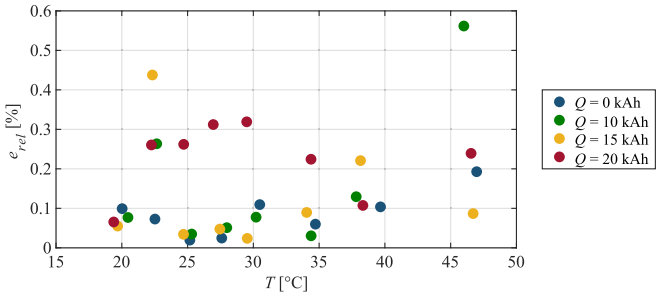

Fig. 9. Percentage relative error of the estimated battery capacity using Eq. (6).

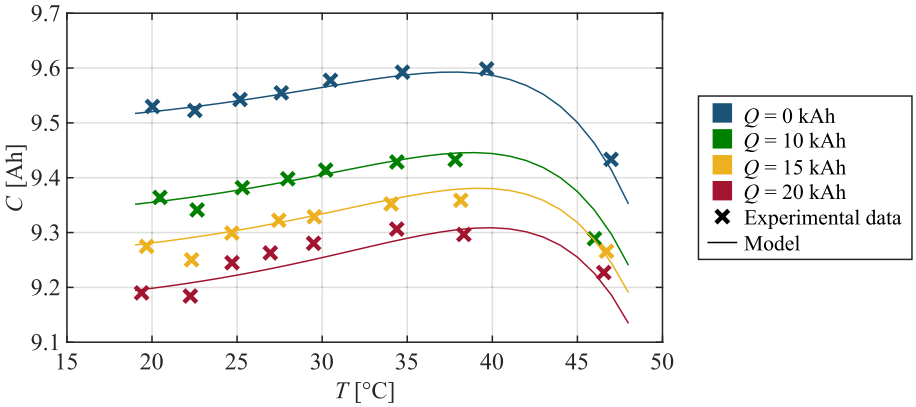

Fig. 8. Experimental and modeled capacity as a function of temperature for different cycling levels using Eq. (6).

Decree of April 16th, 2018.

CRediT authorship contribution statement

Simone Barcellona: Conceptualization, Data curation, Formal analysis, Investigation, Methodology, Validation, Writing – original draft, Writing – review & editing. **Lorenzo Codecasa:** Supervision, Writing – review & editing. **Silvia Colnago:** Data curation, Methodology, Validation, Writing – original draft, Writing – review & editing. **Christian Laurano:** Conceptualization, Formal analysis, Investigation, Writing – review & editing. **Luigi Piegari:** Resources, Supervision, Writing – review & editing. **Sergio Toscani:** Conceptualization, Formal analysis, Investigation, Writing – review & editing.

Declaration of competing interest

The authors declare that they have no known competing financial interests or personal relationships that could have appeared to influence the work reported in this paper.

Data availability

The authors are unable or have chosen not to specify which data has been used.

References

[1] M.A. Divakaran, M. Minakshi, P.A. Bahri, S. Paul, P. Kumari, A.M. Divakaran, K. N. Manjunatha, Rational design on materials for developing next generation lithium-ion secondary battery, Prog. Solid State Chem. 62 (2021) 100298, https://doi.org/10.1016/j.progsolidstchem.2020.100298.

[2] T.B. Reddy, D. Linden, Linden's Handbook of Batteries, Fourth ed., McGraw-Hill Education, New York, NY, 2011.

[3] C. Liu, F. Li, L.-P. Ma, H.-M. Cheng, Advanced materials for energy storage, Adv. Mater. 22 (2010) E28–E62, https://doi.org/10.1002/adma.200903328.

[4] L. Lu, X. Han, J. Li, J. Hua, M. Ouyang, A review on the key issues for lithium-ion battery management in electric vehicles, J. Power Sources 226 (2013) 272–288, https://doi.org/10.1016/j.jpowsour.2012.10.060.

[5] Y. Wang, H. Li, P. He, E. Hosono, H. Zhou, Nano active materials for lithium-ion batteries, Nanoscale 2 (2010) 1294, https://doi.org/10.1039/c0nr00068j.

[6] M.C. Smart, B.V. Ratnakumar, L.D. Whitcanack, F.J. Puglia, S. Santee, R. Gitzendanner, Life verification of large capacity Yardney Li-ion cells and batteries in support of NASA missions, Int. J. Energy Res. 34 (2010) 116–132, https://doi.org/10.1002/er.1653.

[7] I. Bloom, B. Cole, J. Sohn, S. Jones, E. Polzin, V. Battaglia, G. Henriksen, C. Motloch, R. Richardson, T. Unkelhaeuser, D. Ingersoll, H. Case, An accelerated calendar and cycle life study of Li-ion cells, J. Power Sources 101 (2001) 238–247, https://doi.org/10.1016/S0378-7753(01)00783-2.

[8] R. Wright, C. Motloch, J. Belt, J. Christophersen, C. Ho, R. Richardson, I. Bloom, S. Jones, V. Battaglia, G. Henriksen, T. Unkelhaeuser, D. Ingersoll, H. Case, S. Rogers, R. Sutula, Calendar- and cycle-life studies of advanced technology development program generation 1 lithium-ion batteries, J. Power Sources 110 (2002) 445–470, https://doi.org/10.1016/S0378-7753(02)00210-0.

[9] M. Berecibar, I. Gandiaga, I. Villarreal, N. Omar, J. Van Mierlo, P. Van den Bossche, Critical review of state of health estimation methods of Li-ion batteries for real applications, Renew. Sustain. Energy Rev. 56 (2016) 572–587, https://doi.org/10.1016/j.rser.2015.11.042.

[10] S. Barcellona, L. Piegari, Lithium ion battery models and parameter identification techniques, Energies 10 (2017) 2007, https://doi.org/10.3390/en10122007.

[11] Y. Zheng, Z. Shi, D. Guo, H. Dai, X. Han, A simplification of the time-domain equivalent circuit model for lithium-ion batteries based on low-frequency electrochemical impedance spectra, J. Power Sources 489 (2021) 229505, https://doi.org/10.1016/j.jpowsour.2021.229505.

[12] Yoon-Ho Kim, Hoi-Doo Ha, Design of interface circuits with electrical battery models, IEEE Trans. Ind. Electron. 44 (1997) 81–86, https://doi.org/10.1109/41.557502.

[13] M. Dürr, A. Cruden, S. Gair, J.R. McDonald, Dynamic model of a lead acid battery for use in a domestic fuel cell system, J. Power Sources 161 (2006) 1400–1411, https://doi.org/10.1016/j.jpowsour.2005.12.075.

[14] J.E.B. Randles, Kinetics of rapid electrode reactions, Discuss. Faraday Soc. 1 (1947) 11, https://doi.org/10.1039/df9470100011.

[15] S.S. Zhang, K. Xu, T.R. Jow, Electrochemical impedance study on the low temperature of Li-ion batteries, Electrochim. Acta 49 (2004) 1057–1061, https://doi.org/10.1016/j.electacta.2003.10.016.

[16] S. Buller, M. Thele, R.W.A.A. DeDoncker, E. Karden, Impedance-based simulation models of supercapacitors and Li-ion batteries for power electronic applications, IEEE Trans. Ind. Appl. 41 (2005) 742–747, https://doi.org/10.1109/TIA.2005.847280.

[17] IEEE, IEEE Std 450-2020: IEEE Recommended Practice for Maintenance, Testing, and Replacement of Vented Lead-Acid Batteries for Stationary Applications, 2021, pp. 1–71.

[18] J. Jiang, C. Zhang, Fundamentals and Applications of Lithium-ion Batteries in Electric Drive Vehicles, Wiley, 2015, https://doi.org/10.1002/9781118414798.

[19] International Electrotechnical Commission, IEC-62660-2: Secondary Lithium-Ion Cells for the Propulsion of Electric Road Vehicles—Part 2: Reliability and Abuse Testing, 2018.

[20] ISO, ISO 12405-3: ISO Electrically Propelled Road Vehicles—Test Specification for Lithium-Ion Traction Battery Packs and Systems—Part 3: Safety Performance Requirements, 2018.

[21] S. Wang, T. Wu, H. Xie, C. Li, J. Zhang, L. Jiang, Q. Wang, Effects of current and ambient temperature on thermal response of lithium ion battery, Batteries 8 (2022) 203, https://doi.org/10.3390/batteries8110203.

[22] S. Lv, X. Wang, W. Lu, J. Zhang, H. Ni, The influence of temperature on the capacity of lithium ion batteries with different anodes, Energies 15 (2021) 60, https://doi.org/10.3390/en15010060.

[23] C. Chang, Factors affecting capacity design of lithium-ion stationary batteries, Batteries 5 (2019) 58, https://doi.org/10.3390/batteries5030058.

[24] X. Wang, Y. Zhang, H. Ni, S. Lv, F. Zhang, Y. Zhu, Y. Yuan, Y. Deng, Influence of different ambient temperatures on the discharge performance of square ternary lithium-ion batteries, Energies 15 (2022) 5348, https://doi.org/10.3390/en15155348.

[25] P. Keil, S.F. Schuster, J. Wilhelm, J. Travi, A. Hauser, R.C. Karl, A. Jossen, Calendar aging of lithium-ion batteries, J. Electrochem. Soc. 163 (2016) A1872–A1880, https://doi.org/10.1149/2.0411609jes.

[26] S.S. Choi, H.S. Lim, Factors that affect cycle-life and possible degradation mechanisms of a Li-ion cell based on $LiCoO_2$, J. Power Sources 111 (2002) 130–136, https://doi.org/10.1016/S0378-7753(02)00305-1.

[27] R. Wright, J. Christophersen, C. Motloch, J. Belt, C. Ho, V. Battaglia, J. Barnes, T. Duong, R. Sutula, Power fade and capacity fade resulting from cycle-life testing of advanced technology development program lithium-ion batteries, J. Power Sources 119–121 (2003) 865–869, https://doi.org/10.1016/S0378-7753(03)00190-3.

[28] K. Asakura, M. Shimomura, T. Shodai, Study of life evaluation methods for Li-ion batteries for backup applications, J. Power Sources 119–121 (2003) 902–905, https://doi.org/10.1016/S0378-7753(03)00208-8.

[29] F. Leng, C.M. Tan, M. Pecht, Effect of temperature on the aging rate of Li ion battery operating above room temperature, Sci. Rep. 5 (2015) 12967, https://doi.org/10.1038/srep12967.

[30] L. Bodenes, R. Naturel, H. Martinez, R. Dedryvère, M. Menetrier, L. Croguennec, J.-P. Pérès, C. Tessier, F. Fischer, Lithium secondary batteries working at very high temperature: capacity fade and understanding of aging mechanisms, J. Power Sources 236 (2013) 265–275, https://doi.org/10.1016/j.jpowsour.2013.02.067.

[31] J. Yi, U.S. Kim, C.B. Shin, T. Han, S. Park, Modeling the temperature dependence of the discharge behavior of a lithium-ion battery in low environmental temperature, J. Power Sources 244 (2013) 143–148, https://doi.org/10.1016/j.jpowsour.2013.02.085.

[32] A. Fly, I. Kirkpatrick, R. Chen, Low temperature performance evaluation of electrochemical energy storage technologies, Appl. Therm. Eng. 189 (2021) 116750, https://doi.org/10.1016/j.applthermaleng.2021.116750.

[33] S. Barcellona, M. Brenna, F. Foiadelli, M. Longo, L. Piegari, Analysis of ageing effect on Li-polymer batteries, Sci. World J. 2015 (2015) 1–8, https://doi.org/10.1155/2015/979321.

[34] S. Barcellona, L. Piegari, Effect of current on cycle aging of lithium ion batteries, J. Energy Storage 29 (2020) 101310, https://doi.org/10.1016/j.est.2020.101310.

[35] S. Barcellona, S. Colnago, G. Dotelli, S. Latorrata, L. Piegari, Aging effect on the variation of Li-ion battery resistance as function of temperature and state of charge, J. Energy Storage 50 (2022) 104658, https://doi.org/10.1016/j. est.2022.104658.

[36] O. Capron, J. Jaguemont, R. Gopalakrishnan, P. Van den Bossche, N. Omar, J. Van Mierlo, Impact of the temperature in the evaluation of battery performances during long-term cycling—characterisation and modelling, Appl. Sci. 8 (2018) 1364, https://doi.org/10.3390/app8081364.

[37] Y. Zhang, C.-Y. Wang, X. Tang, Cycling degradation of an automotive $LiFePO_4$ lithium-ion battery, J. Power Sources 196 (2011) 1513–1520, https://doi.org/10.1016/j.jpowsour.2010.08.070.

[38] Y. Zhang, C.-Y. Wang, Cycle-life characterization of automotive lithium-ion batteries with $LiNiO_2$ cathode, J. Electrochem. Soc. 156 (2009) A527, https://doi.org/10.1149/1.3126385.

[39] A. Fly, B. Wimarshana, I. Bin-Mat-Arishad, M. Sarmiento-Carnevali, Temperature dependency of diagnostic methods in lithium-ion batteries, J. Energy Storage 52 (2022) 104721, https://doi.org/10.1016/j.est.2022.104721.

[40] A. Hentunen, T. Lehmuspelto, J. Suomela, Time-domain parameter extraction method for Thévenin-equivalent circuit battery models, IEEE Trans. Energy Convers. 29 (2014) 558–566, https://doi.org/10.1109/TEC.2014.2318205.

[41] B.V. Ratnakumar, M.C. Smart, L.D. Whitcanack, R.C. Ewell, The impedance characteristics of Mars Exploration Rover Li-ion batteries, J. Power Sources 159 (2006) 1428–1439, https://doi.org/10.1016/j.jpowsour.2005. 11.085.

[42] M. Mahmud, K.S. Rahman, M. Rokonuzzaman, A.K.M.A. Habib, M.R. Islam, S.M. A. Motakabber, S. Channumsin, S. Chowdhury, Lithium-ion battery thermal

management for electric vehicles using phase change material: a review, Results Eng. 20 (2023) 101424, https://doi.org/10.1016/j.rineng.2023.101424.
[43] M. Uno, K. Tanaka, Influence of high-frequency charge–discharge cycling induced by cell voltage equalizers on the life performance of lithium-ion cells, IEEE Trans. Veh. Technol. 60 (2011) 1505–1515, https://doi.org/10.1109/TVT.2011.2127500.
[44] S. Ma, M. Jiang, P. Tao, C. Song, J. Wu, J. Wang, T. Deng, W. Shang, Temperature effect and thermal impact in lithium-ion batteries: a review, Prog. Nat. Sci. Mater. Int. 28 (2018) 653–666, https://doi.org/10.1016/j.pnsc.2018.11.002.